Soft Matter

Particle Entrainment in Dead-End Pores by Diffusiophoresis

Journal:	*Soft Matter*
Manuscript ID	SM-ART-02-2019-000427.R1
Article Type:	Paper
Date Submitted by the Author:	02-Apr-2019
Complete List of Authors:	Battat, Sarah; Harvard University, Ault, Jesse; Oak Ridge National Laboratory, Computational Sciences and Engineering Division Shin, Sangwoo; University of Hawai'i at Manoa, Department of Mechanical Engineering Khodaparast, Sepideh; Imperial College London Department of Chemical Engineering and Chemical Technology, ; Stone, Howard; Princeton, Mechanical and Aerospace Engineering

SCHOLARONE™
Manuscripts

Soft Matter

ARTICLE TYPE

Particle Entrainment in Dead-End Pores by Diffusiophoresis†

Sarah Battat,[a‡] Jesse T. Ault,[b§] Sangwoo Shin,[c] Sepideh Khodaparast,[b¶] and Howard A. Stone[b*]

The transport of particulate matter to and from dead-end pores is difficult to achieve due to confinement effects. Diffusiophoresis is a phenomenon that results in the controlled motion of colloids along solute concentration gradients. Thus, by establishing an electrolyte concentration gradient within dead-end pores, it is possible to induce the flow of particles into and out of the pores via diffusiophoresis, as has been demonstrated recently. In this paper, we explain the pore-scale mechanism by which individual colloids are entrained in dead-end pores by diffusiophoresis. We flow particles past a series of dead-end pores in the presence of a solute concentration gradient. Our results reveal that particles execute pore-to-pore hops before ultimately being captured. We categorize an event as *particle capture* when the particle's trajectory terminates within the dead-end pore. Experiments and numerical simulations demonstrate that particle capture only occurs when flowing particles are positioned sufficiently close to the pore entry. Outside this capture region, the particles have insufficient diffusiophoretic velocities to induce capture and their dynamics are largely dominated by their free-stream advective velocities. We observe that the particles move closer to the device wall as they hop, thereby reducing the effect of flow advection and increasing that of diffusiophoresis. These results enhance our understanding of suspension dynamics in a driven system and have implications for the development, design, and optimization of diffusiophoretic platforms for drug delivery, cosmetics, and material recovery.

1 Introduction

Diffusiophoresis refers to the controlled movement of particles along a solute concentration gradient.[1,2] This transport technique was discovered and initially employed in industry to coat substrates with latex and to deposit paint films on metal automobile parts.[3,4] Recent studies reveal an array of new applications of diffusiophoresis for enhanced fabric cleaning in laundry processes,[5] preconcentration of biomolecules for rapid assays,[6,7] recovery of oil droplets from rock fissures,[8] membraneless water purification,[9,10] amongst others[11–14]. For example, diffusiophoresis enables the insertion or removal of particulate matter (dirt, biomolecules, or drops) in confined, dead-end geometries. Despite its importance, the pore-scale process of individual particle entrainment in dead-end pores by diffusiophoresis has yet to be studied.

Here, we use experiments and numerical simulations to study the mechanism by which individual particles are entrained in dead-end pores via diffusiophoresis. As illustrated in Figure 1, we consider a system in which a low concentration electrolyte solution (0.1 mM sodium chloride) containing fluorescent polystyrene particles (0.01% by volume and one micron in diameter) flows past a series of pores containing the same electrolyte solution, albeit at a higher initial concentration (10 mM sodium chloride). The velocity of an individual particle ($\mathbf{u}$) consists of two components, namely that due to diffusiophoresis ($\mathbf{u}_d$) and that due to fluid advection ($\mathbf{u}_f$). The diffusiophoretic velocity of a particle is defined as

$$\mathbf{u}_d = \Gamma_d \boldsymbol{\nabla} \ln C, \tag{1}$$

where $C(\mathbf{x}, t)$ is the solute concentration with temporal (t) and spatial ($\mathbf{x}$) dependence and Γ_d is the diffusiophoretic mobility of the particle, which for symmetric electrolytes and in the limit of

[a] Department of Physics, Princeton University, Princeton, New Jersey 08544

[‡] Present address: John A. Paulson School of Engineering and Applied Sciences, Harvard University, Cambridge, Massachusetts 02138

[b] Department of Mechanical and Aerospace Engineering, Princeton University, Princeton, New Jersey 08544

[§] Present address: Computational Sciences and Engineering Division, Oak Ridge National Laboratory, Oak Ridge, Tennessee 37831

[c] Department of Mechanical Engineering, University of Hawaii at Manoa, Honolulu, Hawaii 96822

[¶] Present address: Department of Chemical Engineering, Imperial College London SW7 2AZ, United Kingdom

[*] hastone@princeton.edu

[†] Electronic Supplementary Information (ESI) available.
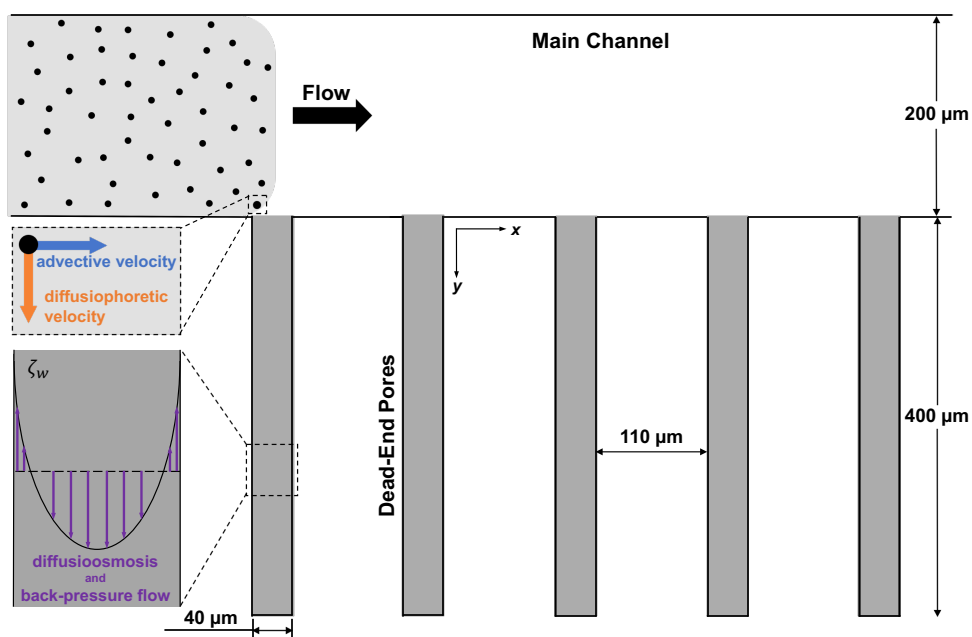
Fig. 1 Transport of colloidal particles by diffusiophoresis for our experimental system with a negative value of β. A suspension of polystyrene particles in a low concentration salt solution flows through an evacuated main channel and past a series of dead-end pores containing a higher concentration salt solution. (inset) The particle velocities have two components, namely that due to fluid advection and that due to diffusiophoresis. Within the dead-end pores, the flow profile is parabolic owing to a combination of pressure-driven back-flow and diffusioosmosis along the walls of the channel.

a thin Debye layer, is given by

$$\Gamma_d = \frac{\varepsilon k_B T}{\mu z e}\left[\beta \zeta_p + \frac{4k_B T}{ze}\ln\left(\cosh\left(\frac{ze\zeta_p}{4k_B T}\right)\right)\right], \qquad (2)$$

where ε represents the permittivity of the medium, T is the absolute temperature, μ is the dynamic viscosity of the solution, z is the valence of the electrolyte, e is the elementary charge, k_B is the Boltzmann constant, ζ_p is the zeta potential of the particle, and $\beta = (D_+ - D_-)/(D_+ + D_-)$ is the relative ratio of the diffusivities of the cationic (D_+) and anionic (D_-) species in solution.[2]

There are two contributions to the diffusiophoretic mobility of a particle in a binary electrolyte, namely electrophoresis and chemiphoresis, which correspond, respectively, to the first and second terms on the right-hand side of Equation (2). When suspended in an electrolyte solution, the fluorescent polystyrene particles acquire a surface charge.[15] Within the Debye layer, the surface charge is screened by excess counter-ions in solution. In the presence of a macroscopic concentration gradient and owing to the different diffusivities of the co- and counter-ions, a local electric field arises and its direction is prescribed by the sign of β in Equation (2). This electric field leads to fluid flow within the Debye layer and particle propulsion in the opposite direction, which is electrophoresis. Particles also experience an osmotic pressure imbalance due to the solute gradient; chemiphoresis refers to the resultant particle propulsion towards the region of higher solute concentration.[2,15]

As illustrated in the inset in Figure 1, the flow profile within a dead-end pore is approximately parabolic owing to a combination of wall-driven diffusioosmosis and pressure-driven back-flow. The former contribution results in a slip velocity along the pore

walls directed in the negative y-direction for our concentration gradient choice; we differentiate this effect from diffusiophoresis by the immobility of the device walls.[8,15] Meanwhile, the latter phenomenon arises due to the zero-net-mass-flux condition in the dead-end pore. The fluid flow direction along the central axis of the pore opposes that of the diffusioosmotic flow. The combination of these effects results in a recirculating flow profile within the pore, which will be illustrated by numerical simulation below in Figure 3B.[8]

2 Methods

Experiments are performed in a microfluidic device of the kind sketched in Figure 1. The device is made by mixing polydimethylsiloxane (PDMS) with a curing agent (Dow Corning, Sylgard® 184) in a ratio of 5:1 by weight and cross-linking the mixture on a photolithographically patterned silicon wafer mold. Subsequently, we peel back the cast PDMS and plasma-bond it to a slab of neat PDMS. The out-of-plane thickness of all channels and dead-end pores is approximately $\ell = 10$ μm and the width of the dead-end pores is $w = 40$ μm. Prior to use, the device is saturated overnight in water under vacuum to prevent any permeation of fluid from the main channel or dead-end pores into the bulk PDMS slab. In our system, the pore walls made of PDMS have zeta potentials of $\zeta_w \approx -30$ mV.[15]

Orange fluorescent polystyrene particles with a diameter of one micron (FluoSpheres™, Thermo Fisher Scientific) and a density of $\rho = 1.055$ g/cm^3 are suspended in a solution of 0.1 mM sodium chloride (Sigma-Aldrich) at a concentration of 0.01% by volume. In some control experiments, orange carboxylate-modified fluorescent polystyrene particles (FluoSpheres™, Thermo Fisher Scientific) with a diameter of 0.2 μm and a density of

$\rho = 1.055$ g/cm^3 are employed instead. Although polystyrene is slightly more dense than the surrounding liquid, sedimentation does not play a significant role in our set-up, since the scale heights for both one micron and 0.2 μm particles are greater than the channel height. In our experiments, the polystyrene particles have zeta potentials of $\zeta_p \approx -70$ mV.[15]

Initially, a solution of 10 mM sodium chloride is prepared and injected into the device. Manual, pulsating pressure is applied to the device to establish a homogeneous solute concentration within the dead-end pores. Our choice of the initial solute concentration gradient for the study of particle entrainment in dead-end pores is dictated by the fact that $\beta \approx -0.21$ for sodium chloride, meaning that negatively-charged polystyrene particles move towards regions with a higher solute concentration.[2,16] The main channel is then evacuated with an air-filled syringe to ensure a step boundary condition in both the salt and particle concentrations upon the commencement of continuous flow in the main channel. The particle-laden solution is flowed through the main channel; the flow rate is controlled with a syringe pump (Pump 11 Pico Plus Elite, Harvard Apparatus). The fluorescent particles are visualized with an inverted fluorescence microscope (DMI4000B, Leica) and their motion is recorded with a microscope camera (DFC 360 FX, Leica) or a high-speed camera (Phantom v7.3, Vision Research). For the analysis of individual particle trajectories, particle tracking software is used.[17] Particle image velocimetry analysis of the high-speed recordings is also performed.[‡‡] General image processing is carried out in Fiji, an open-source platform for image analysis.[18]

Three-dimensional numerical simulations of particle trajectories are computed with OpenFOAM, an open-source computational fluid dynamics toolbox.[19] We develop a customized solver based on the `simpleFoam` and `scalarTransportFoam` solvers in OpenFOAM.[20] We assume that the flow is quasi-steady with respect to the particle dynamics because the kinematic viscosity is much greater than both the salt and particle diffusivities, and the Reynolds number is low, where the Reynolds number Re $= \rho u \ell / \mu$ is defined as the ratio of the inertial to viscous forces given a fluid density ρ, a characteristic fluid velocity u, a characteristic length ℓ (here $\ell = 10$ μm), and a fluid viscosity μ. Predicated upon this separation of timescales, our solver iterates the calculation of the quasi-steady fluid flow with the `SIMPLE` algorithm. Subsequently, it updates the solute concentration by integrating an advection-diffusion equation. The characteristic Peclet number in the main channel is Pe $= \mathscr{O}(100)$, where the Peclet number Pe $= w_c u / D_s$ denotes the ratio of advection to diffusion in the main channel for a channel width w_c (here $w_c = 200$ μm), a characteristic fluid velocity u, and an effective salt diffusivity D_s (as defined in Equation (4) below). Our simulation accounts for the diffusioosmotic effects along the pore walls; we implement these boundary conditions using the `groovyBC` boundary condition utility provided by `swak4Foam`. We calculate the trajectory of an individual particle, which is advected as a point particle, by integrating its instantaneous velocity field in time, where the velocity field is the sum of

the fluid velocity $(\mathbf{u}_f)$ and the particle's diffusiophoretic velocity $(\mathbf{u}_d)$.

In our OpenFOAM simulations of the experimental configuration, we use second-order spatial discretization schemes and first-order integration in time. We specify a spatial tolerance of 0.5 μm for the solver. The system evolves in time given initial conditions of zero fluid velocity and specified high and low solute concentrations, respectively, within the pore and the main channel. As per Figure 1, along the main channel inlet, we specify a constant mean fluid velocity and a normal pressure gradient of zero. Moreover, we set the solute concentration to a constant, low value along the inlet. At all points along the main channel outlet, we assign zero values to the pressure and the fluid velocity's normal gradient; the latter condition assumes that the flow is fully developed at the outlet. At the outlet, the normal gradient of the solute concentration is zero. We enforce the no-flux condition along the channel walls by assigning the normal gradient of the solute concentration a value of zero (refer to the Supplementary Information[†] for further simulation details).

We also simulate the flow field of our system with a custom-designed solver in MATLAB using an incompressible vorticity/streamfunction formulation.[21] In systems such as ours where the depth-wise dimension of the microfluidic device is small ($\ell \ll w, w_c$), the Brinkman approximation, introduced in Equation (3), allows us to approximate the three-dimensional flow as the flow averaged along the depth-wise direction. In this limit and assuming steady-state low Reynolds number flow, the governing flow equation simplifies to

$$0 = -\boldsymbol{\nabla}_{\perp} p + \mu \nabla_{\perp}^2 \overline{\mathbf{u}} - \frac{\mu}{k} \overline{\mathbf{u}}, \tag{3}$$

where $\overline{\mathbf{u}}$ is the depth-averaged fluid velocity, μ is the viscosity of the particle-laden electrolyte solution (approximately that of water), $k = \ell^2/12$ is the effective permeability of the medium which depends upon the channel depth, ℓ is the depth of the channel (here $\ell = 10$ μm), $\boldsymbol{\nabla}_{\perp}$ is the gradient in the direction perpendicular to the channel height (here $\boldsymbol{\nabla}_{\perp} = \hat{\boldsymbol{x}}\partial/\partial x + \hat{\boldsymbol{y}}\partial/\partial y$ in accordance with the coordinate system introduced in Figure 1), and p is the pressure.[22,23] Equation (3) is solved along with the continuity equation, $\boldsymbol{\nabla} \cdot \overline{\mathbf{u}} = 0$. We recover excellent agreement between the results of the Brinkman approximation simulation (Figure 3B) and the three-dimensional OpenFOAM simulation (Supplementary Information[†], Figure S1B). Thus, in the interests of computational simplicity and efficiency, we resort to this two-dimensional simulation method because it captures the essence of three-dimensional effects while saving computing power, time, and resources and allows us to readily make quantitative comparisons with the experiments.

In the MATLAB simulation, we partition the geometry of interest into a 2 μm $\times$ 2 μm mesh grid. We impose diffusioosmotic boundary conditions along the lateral pore walls and assume a fully developed Poiseuille flow at both the inlet and outlet of the main channel. Moreover, we apply the no-flux condition along the device's boundaries. As is the case for our OpenFOAM simulation, the separation of timescales allows us to iteratively solve for the quasi-steady-state flow and update the solute concentra-

---

‡‡ JPIV Particle Image Velocimetry software, version 2.1 (2008).
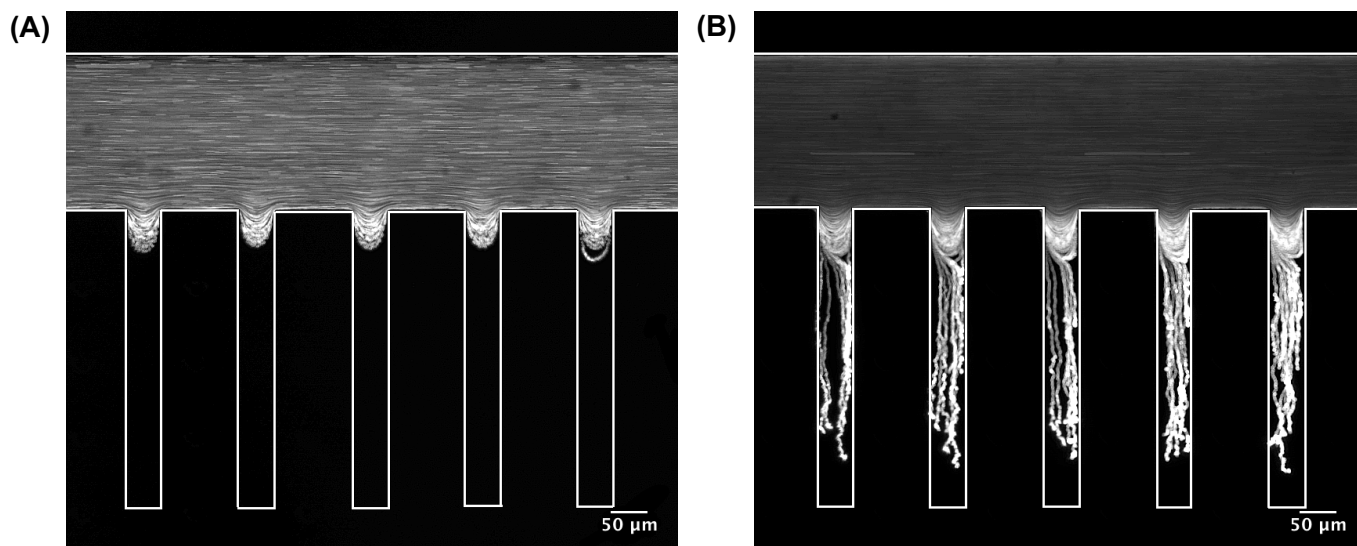
Fig. 2 The entrainment of individual, one-micron diameter particles in dead-end pores by diffusiophoresis. (A) In the absence of an electrolyte concentration gradient, though particles penetrate the dead-end pores, they are not entrained therein as illustrated by this time-stack of high exposure fluorescent images. (B) In the presence of a sodium chloride concentration gradient (in which the initial concentration of sodium chloride is 0.1 mM outside the pore and 10 mM inside the pore), the particles experience diffusiophoresis and migrate towards the higher concentration region and into the dead-end pores. The particle tracks in the main channel are fainter than those in (A) due to a difference in contrast settings during image processing.

tion by transiently solving the solute advection-diffusion equation. In turn, the velocity is determined from the vorticity and streamfunction, where $\overline{\mathbf{u}} = (\overline{u}_x, \overline{u}_y)$ is the depth-averaged fluid velocity, $\nabla_\perp^2 \psi = -\omega$ is an elliptic equation that relates the streamfunction (ψ) to the vorticity (ω), and $\omega = \partial \overline{u}_y / \partial x - \partial \overline{u}_x / \partial y$ is the vorticity in the depth-wise direction (refer to the Supplementary Information[†] for further simulation details).

3   Results and Discussion

It is well-documented in the literature that particles of various sizes undergo diffusiophoresis for a wide range of solute concentration gradients.[2,4,15,24,25] Since the primary purpose of this study is to understand the process of individual particle entrainment in dead-end pores by diffusiophoresis, our experiments are conducted using a single electrolyte concentration difference and (in large part) a fixed particle size. In doing so, we seek to eliminate extraneous effects on our system and focus on the characterization of the entrainment mechanism at the pore scale.

Experiments confirm that *particle capture* does not occur in the absence of an electrolyte gradient, as shown in Figure 2A. Particle capture designates the successful entrainment of a particle in a dead-end pore, meaning that the particle's trajectory terminates within the pore. It is clear, however, that the particles can *penetrate* the opening of the pore without being captured, i.e., the particles move into the pore by hydrodynamics alone, but ultimately escape. In the presence of an electrolyte gradient, particle capture takes place as depicted in Figure 2B. These particles are advected by the main channel flow and are also subject to diffusiophoresis.

The results in Figure 2B suggest that, even under the action of diffusiophoresis, many particles that penetrate the dead-end pores are not actually captured. In Figure 3A, we plot the maximum pore penetration depth without capture (scaled by the pore width) as a function of the Reynolds number in the main channel. The penetration depth corresponds to the vertical distance between the bottom wall of the main channel and the apex of the (closed) quasi-parabolic particle pathline within the pore. Since the Reynolds numbers probed in this experiment are of order $\mathrm{Re} = \mathscr{O}(10^{-2})$, as expected, the penetration depth is independent of the Reynolds number. Moreover, the penetration depth remains constant in the absence of a solute concentration gradient and in experiments where approximately neutrally buoyant tracer particles (0.2 μm in diameter), which presumably follow the fluid streamlines, are used. Our two-dimensional, Brinkman-model MATLAB simulation reveals a deep penetration of fluid streamlines in the dead-end pore in the presence of an electrolyte concentration gradient (Figure 3B). In the absence of a solute concentration gradient, we also observe deeply penetrating fluid streamlines (Supplementary Information[†], Figure S1A). The experimental and numerical results suggest that particle penetration into a pore without capture is a feature of the flow geometry rather than being due to diffusiophoresis.

We also note that the penetrating streamlines are asymmetric (Figure 3B). The Peclet number at the pore entry is on the order of $\mathrm{Pe} = \mathscr{O}(20)$. Fluid advection dominates diffusion at the pore entry; the main channel flow sweeps fluid near the pore mouth such that the solutes are redistributed unevenly and a lateral solute concentration gradient arises (Supplementary Information[†], Figure S2).

We provide sample trajectories (namely y-displacements) of one-micron diameter particles that are captured in pores at a Reynolds number of $\mathrm{Re} = 0.028$ in Figure 4A; the particle displacements are measured relative to the initially-tracked positions. In general, the particles execute a sequence of pore-to-pore hops (represented by the quasi-parabolic portions of the y-displacement plot) until they are fully entrained in the pore. The

(A)

(B)

(C)
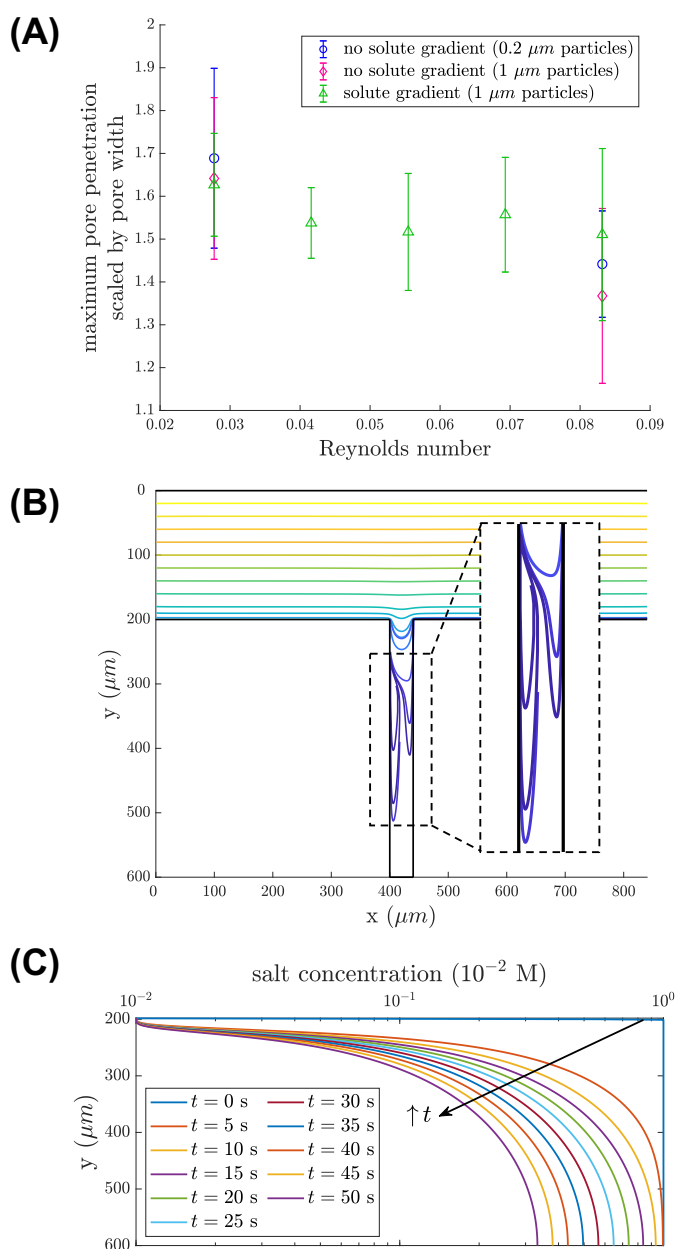
Fig. 3 Flow profile within a dead-end pore in the presence of a sodium chloride concentration difference. (A) Plot of the maximum pore penetration distance (without capture) of a particle scaled by the pore width ($w = 40\ \mu m$) as a function of the Reynolds number. The Reynolds number is changed by altering the injection flow rate at the inlet. (B) Two-dimensional simulation of the streamlines within the dead-end pore by the Brinkman approximation at time $t = 10\ seconds$ after the commencement of the experiment, where each streamline is assigned a separate color. Recirculation currents due to diffusioosmosis and pressure-driven flow within the pore are observed. (C) OpenFOAM simulation of the time evolution of the concentration field within the dead-end pore, where (in accordance with (B)) $y = 200\ \mu m$ corresponds to the top of the pore and $y = 600\ \mu m$ to its bottom. The concentration is sampled along the center-line of the pore and at its mid-plane in the depth-wise direction.

term *hop* designates a particle's penetration in a dead-end pore and its eventual escape therefrom. These hopping segments are separated by plateau regions, which correspond to periods of time

when a particle moves close to the bottom wall of the main channel with negligible changes in its vertical y-displacement.

Upon connecting the plateau regions (black dots) in Figure 4A, we note a consistent trend whereby particles move closer to the bottom wall of the main channel (corresponding to an increase in their y-displacement) as they carry out more hops; we underscore this trend in the upper-right inset of Figure 4A. Diffusiophoresis drives particles further into the dead-end pore than they would normally travel in the absence of a solute concentration gradient. This effect causes particles to cross fluid streamlines within the pore and to emerge from the pore approximately along streamlines that penetrated the pore more deeply and are closer to the bottom wall of the main channel than the particle's pre-hop position. Due to negligible diffusioosmotic effects in the main channel, we assume a no-slip boundary condition along the main channel walls and, thus, a decay of the velocity to zero at the walls. In fact, at a Reynolds number of Re = 0.028, a particle whose radius is five percent of the channel depth and 1.25% of the pore width located one micron from the bottom main channel wall moves at roughly 25% of its velocity at the channel's axis of symmetry (Supplementary Information[†], Figure S3). It follows that the advective velocity of an emergent particle decreases with each hop and, in time, the diffusiophoretic velocity is sufficiently large for particle capture to ensue.

We supplement our quantitative analysis of particle motion with visualizations of experimental and simulated particle trajectories. In Figure 4B, we plot the particle pathlines, which are color-matched to the y-displacement curves in Figure 4A. We simulate the particle trajectories in OpenFOAM and obtain the results in Figure 4C. We observe excellent agreement between the experimental and simulated results. We confirm that one-micron diameter particles are only entrained in the dead-end pores if they originate from positions (approximately) less than or equal to two microns from the bottom main channel wall. This finding confirms our earlier hypothesis whereby the effect of main channel fluid advection lessens as the particles execute more pore-to-pore hops. Our simulation results also reflect the empirical observation that captured particles are initially entrained along the left side of a dead-end pore before moving towards the center of the pore. As mentioned previously, due to the large Peclet number (Pe = $\mathscr{O}(20)$) at the pore entry, advection sweeps the low concentration electrolyte solution from the main channel into the dead-end pore, which contains a high concentration electrolyte solution. Thus, at the pore's opening, there is an increasing concentration gradient along the pore's width as shown in Figure S2 (Supplementary Information[†]). This phenomenon accounts for the asymmetric rightwards motion of the particle when captured.

We also note that the hopping signature before capture persists in time. The effective diffusivity of a binary salt is given by

$$D_s = \frac{2 D_+ D_-}{D_+ + D_-}, \tag{4}$$

where D_+ and D_- are the diffusion coefficients of the cationic and anionic species, respectively.[2] In our system, we estimate that the diffusivity of sodium chloride is $D_s \approx 1.6 \times 10^{-9}$ m^2/s.[16] It follows that it should take roughly one hundred seconds for

(A)

(B)

(C)
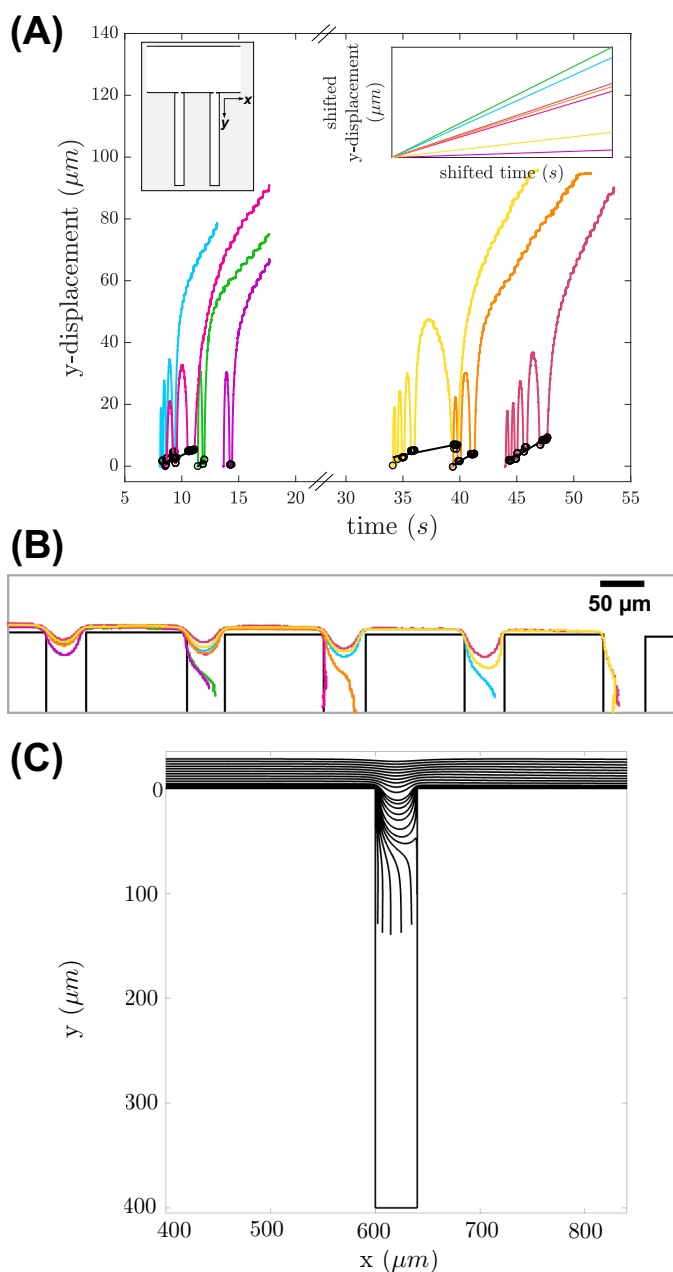
Fig. 4 Particle entrainment mechanism in dead-end pores by diffusiophoresis at $Re = 0.028$. (A) Plot of the *y*-displacements of many one-micron diameter particles as a function of the experimental duration, where the displacement is measured relative to a particle's initially-tracked position and the *y*-direction is oriented along the pore's length. (inset) Magnified view of the lines connecting the plateau regions (denoted by black circles in the main panel) of each particle trajectory, which are shifted to the origin and color-matched according to the color of the corresponding trajectory. (B) Color-matched representation of the experimental particle trajectories in (A), characterized by a series of pore-to-pore hops and eventual capture. (C) OpenFOAM simulation of trajectories of particles released at the commencement of an experiment ($t = 0$) at a lateral distance of $200\ \mu$m from the pore opening subject to diffusiophoresis and advection in the main channel (refer to the Supplementary Information[†] for simulation details).

the electrolyte gradient along the pore's length to reach equilibrium. At this point in time, however, diffusiophoresis still persists

despite the weak electrolyte gradient because the particle's diffusiophoretic velocity is proportional to the gradient of the logarithm of the electrolyte gradient.[12] Our results indicate that the hopping signature before particle capture extends to times well over ninety seconds from the commencement of the experiment (Supplementary Information[†], Figure S4).

4 Conclusion

In conclusion, we propose a mechanism by which individual particles are entrained in dead-end pores by a diffusiophoretic mechanism. Upon flowing polystyrene particles past a series of dead-end pores in the presence of an electrolyte gradient, the particles execute pore-to-pore hops before eventual capture. Through experiments and simulations, we verify that particle entrainment in dead-end pores can only occur when the particle's advective velocity is negligible as compared to its diffusiophoretic velocity. Since the particle crosses streamlines within the pore due to its diffusiophoretic velocity, it exits the pore and moves along the main channel wall at a position closer than that which it occupied prior to the hop. Given the no-slip condition along the solid boundary, the advective velocity decays rapidly normal to the wall. Therefore, there exists a critical (vertical) distance from the pore entry beyond which particles are not captured. Though we employed an increasing concentration gradient (along the *y*-direction) of sodium chloride and negatively-charged polystyrene particles, the experimental parameters could be tuned to maintain the generality of our findings. For instance, in the event that particles with a positive zeta potential were used, sodium chloride could be replaced by a salt with $\beta > 0$ without altering the direction of the gradient to ensure that particles were entrained into the dead-end pores.[2] Thus, this account of individual particle entrainment in dead-end pores by diffusiophoresis enriches our fundamental understanding of suspension dynamics in a system subject to various forces. Moreover, it allows us to improve upon the design of diffusiophoretic platforms for drug delivery, cosmetics, oil recovery, and pore cleaning purposes.

Conflicts of interest

There are no conflicts to declare.

Acknowledgements

References

1 B. V. Derjaguin, G. Sidorenkov, E. Zubashchenko and E. Kiseleva, *Prog. Surf. Sci.*, 1993, **43**, 138–152.

2 D. C. Prieve, J. L. Anderson, J. P. Ebel and M. E. Lowell, *J. Fluid Mech.*, 1984, **148**, 247–269.

3 B. V. Derjaguin, S. S. Dukhin and A. A. Korotkova, *Prog. Surf. Sci.*, 1993, **43**, 153–158.

4 J. L. Anderson and D. C. Prieve, *Sep. Purif. Methods*, 1984, **13**, 67–103.

5 S. Shin, B. Warren, P and H. A. Stone, *Phys. Rev. Appl.*, 2018, **9**, 034012.

6 S. Shin, J. T. Ault, P. B. Warren and H. A. Stone, *Phys. Rev. X*, 2017, **7**, 041038.

7 R. Guha, F. Mohajerani, A. Mukhopadhyay, M. D. Collins, A. Sen and D. Velegol, *ACS Appl. Mater. Interfaces*, 2017, **9**, 43352–43362.

8 A. Kar, T.-Y. Chiang, I. Ortiz Rivera, A. Sen and D. Velegol, *ACS Nano*, 2015, **9**, 746–753.

9 S. Shin, O. Shardt, P. B. Warren and H. A. Stone, *Nat. Commun.*, 2017, **8**, 15181.

10 H. Lee, J. Kim, J. Yang, S. W. Seo and S. J. Kim, *Lab Chip*, 2018, **18**, 1713–1724.

11 J. Palacci, B. Abecassis, C. Cottin-Bizonne, C. Ybert and L. Bocquet, *Phys. Rev. Lett.*, 2010, **104**, 138302.

12 B. Abecassis, C. Cottin-Bizonne, C. Ybert, A. Ajdari and L. Bocquet, *Nat. Mater.*, 2008, **7**, 785–789.

13 S. M. Friedrich, J. M. Burke, K. J. Liu, C. F. Ivory and T.-H. Wang, *Nat. Commun.*, 2017, **8**, 1213.

14 J. T. Ault, P. B. Warren, S. Shin and H. A. Stone, *Soft Matter*, 2017, **13**, 9015–9023.

15 S. Shin, E. Um, B. Sabass, J. T. Ault, M. Rahimi, P. B. Warren and H. A. Stone, *Proc. Natl. Acad. Sci. U.S.A.*, 2016, **113**, 257–261.

16 E. Samson, J. Marchand and K. A. Snyder, *Mater. Struct.*, 2003, **36**, 156–165.

17 I. F. Sbalzarini and P. Koumoutsakos, *J. Struct. Biol.*, 2005, **151**, 182–195.

18 J. Schindelin, I. Arganda-Carreras, E. Frise, V. Kaynig, M. Longair, T. Pietzsch, S. Preibisch, C. Rueden, S. Saalfeld, B. Schmid, J.-Y. Tinevez, D. J. White, V. Hartenstein, K. Eliceiri, P. Tomancak and A. Cardona, *Nat. Methods*, 2012, **9**, 676–682.

19 H. G. Weller, G. Tabor, H. Jasak and C. Fureby, *Comp. Phys.*, 1998, **12**, 620–631.

20 I. E. Barton, *Int. J. Numer. Meth. Fl.*, 1998, **26**, 459–483.

21 G. Tryggvason, *A Finite Difference Code for the Navier-Stokes Equations in Vorticity/Streamfunction Form*, http://www3.nd.edu/~gtryggva/CFD-Course/2011-Lecture-5.pdf, 2011.

22 H. C. Brinkman, *Flow Turbul. Combust.*, 1949, **1**, 27–34.

23 M. Nagel and F. Gallaire, *Comput. Fluids*, 2015, **107**, 272–284.

24 D. Velegol, A. Garg, R. Guha, A. Kar and M. Kumar, *Soft Matter*, 2016, **12**, 4686–4703.

25 D. C. Prieve, S. M. Malone, A. S. Khair, R. F. Stout and M. Y. Kanj, *Proc. Natl. Acad. Sci. U.S.A.*, 2018.

Manuscript ID: SM-ART-02-2019-000427
Title: Particle Entrainment in Dead-End Pores by Diffusiophoresis
Authors: Sarah Battat, Jesse T. Ault, Sangwoo Shin, Sepideh Khodaparast, Howard A. Stone

Table of Contents
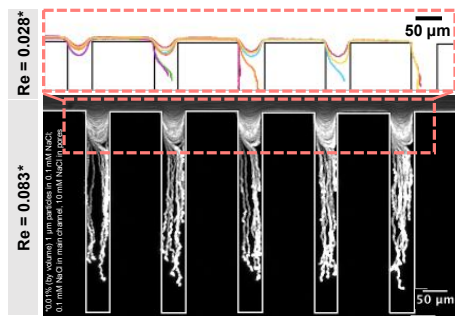
We determine the mechanism by which individual particles cross streamlines to become entrained in dead-end pores by diffusiophoresis.